⌘ *Author's Choice*
THE JOURNAL OF BIOLOGICAL CHEMISTRY VOL. 284, NO. 49, pp. 34272–34282, December 4, 2009

Fibril Fragmentation Enhances Amyloid Cytotoxicity*[S]◆

Received for publication, July 28, 2009, and in revised form, September 22, 2009 Published, JBC Papers in Press, October 6, 2009, DOI 10.1074/jbc.M109.049809

Wei-Feng Xue, Andrew L. Hellewell, Walraj S. Gosal[1], Steve W. Homans, Eric W. Hewitt, and Sheena E. Radford[2]

From the Astbury Centre for Structural Molecular Biology, Institute of Molecular and Cellular Biology, University of Leeds, Leeds LS2 9JT, United Kingdom

Fibrils associated with amyloid disease are molecular assemblies of key biological importance, yet how cells respond to the presence of amyloid remains unclear. Cellular responses may not only depend on the chemical composition or molecular properties of the amyloid fibrils, but their physical attributes such as length, width, or surface area may also play important roles. Here, we report a systematic investigation of the effect of fragmentation on the structural and biological properties of amyloid fibrils. In addition to the expected relationship between fragmentation and the ability to seed, we show a striking finding that fibril length correlates with the ability to disrupt membranes and to reduce cell viability. Thus, despite otherwise unchanged molecular architecture, shorter fibrillar samples show enhanced cytotoxic potential than their longer counterparts. The results highlight the importance of fibril length in amyloid disease, with fragmentation not only providing a mechanism by which fibril load can be rapidly increased but also creating fibrillar species of different dimensions that can endow new or enhanced biological properties such as amyloid cytotoxicity.

Amyloid fibril deposits are associated with numerous disorders, including type II diabetes mellitus and Alzheimer and Parkinson diseases (1). These proteinaceous fibrillar aggregates are commonly regarded as the self-assembly end products of peptides or proteins that form by nucleated polymerization (2). Despite sharing a common cross-β molecular architecture, fibrils of different morphologies and/or superstructural features can be formed, even from the same starting material (3–6). Other types of aggregates, including oligomeric species of different sizes (*e.g.* (25)), typically accumulate during fibril formation. It has also been shown that mechanical stress can affect the products of fibril assembly, producing fibrils of different dimensions and/or molecular structure even under otherwise identical conditions (3, 4, 8).

Because of the enormous complexity and heterogeneity in the dynamic equilibrium between different species populated during amyloid formation, the identity of the culprits of cytotoxicity associated with amyloid disease remains far from clear despite a plethora of studies in recent years (for example, Refs. 9–15). The species involved in mediating the cytotoxicity associated with many amyloid disorders were initially assumed to be fibrils and fibril plaques that are abundant in diseased tissues (16, 17). However, numerous recent reports have focused on soluble prefibrillar oligomers as the primary cytotoxic species (for example, Refs. 9–12). Despite significant evidence supporting prefibrillar oligomeric species as toxic agents, examples of toxicity associated with fibrils persist (*e.g.* Refs. 13, 15, and 18). This raises the possibility that the determinants of cytotoxicity may not always be associated with the same type of species, and for some amyloidogenic proteins, fibrils themselves or fibril-associated species may possess cytotoxic potential (19). Recent studies have shown that Aβ[3] fibrils interacting with sphingolipids, gangliosides, or cholesterol, all of which have been shown to associate with amyloid plaques *in vivo* (20), result in the release of cytotoxic species (14), whereas the assembly process of islet amyloid polypeptide (also known as amylin) fibrils on lipid membranes results in liposome disruption, suggesting fibril-associated toxicity during the fibril growth process (21). Taken together, these studies suggest that fibrils should perhaps not be dismissed as the inert products of amyloid assembly but might provide a further source of toxicity, either directly by interacting with membranes or indirectly by acting as a source of cytotoxic entities.

How fibrils elicit a biological response may not only depend on their chemical composition or molecular properties, but their physical attributes such as length, width, or surface area may also play important roles, as found for other nanoscale materials (22, 23). To investigate this possibility, we report here a detailed analysis of the relation between fibril length, quantified using tapping-mode atomic force microscopy (TM-AFM), and the structural and biological properties of amyloid fibrils. Using long straight (LS) fibrils formed from human β_2-microglobulin (β_2m) (3), we show that samples containing these fibrils can disrupt model liposome membranes and reduce cell viability, whereas prefibrillar oligomeric species formed in the lag phase of assembly and fibrillar aggregates with different

* This work was supported by grants from the Wellcome Trust (Grant 075675) and Biotechnology and Biological Sciences Research Council (Grant BB/526502/1).
⌘ *Author's Choice*—Final version full access.
◆ This article was selected as a Paper of the Week.
[S] The on-line version of this article (available at http://www.jbc.org) contains supplemental Figs. 1 and 2.
[1] Present address: University of Texas Southwestern Medical Center at Dallas, 5323 Harry Hines Blvd., Dallas, TX, 75390.
[2] To whom correspondence should be addressed: Astbury Centre for Structural Molecular Biology, Garstang Bldg., University of Leeds, Leeds LS2 9JT, UK. Tel.: 44-113-343-3170; Fax: 44-113-343-7486; E-mail s.e.radford@leeds.ac.uk.

[3] The abbreviations used are: Aβ, β-amyloid; αSyn, α-synuclein; β_2m, β_2-microglobulin; EM, electron microscopy; FTIR, Fourier transform infrared; LS, long-straight β_2m fibrils; Lyz, lysozyme; RL, rod-like β_2m fibrils; WL, worm-like β_2m fibrils; Sh, short form; Ln, long form; MTT, 3-(4,5-dimethylthiazol-2yl)-2,5-diphenyltetrazolium bromide; ThT, thioflavin T; TM-AFM, tapping mode atomic force microscopy; LUV, large unilamellar vesicles.

structural properties (3, 7) do not. Strikingly, we show that the cytotoxicity displayed by the LS fibril samples is enhanced by reducing fibril length, supporting the idea that the physical dimensions of fibrils can also modulate their cytotoxic potential. The same length-dependent effect is also observed with fibrils formed from lysozyme and α-synuclein, suggesting that reduction of fibril length by fragmentation presents a generic mechanism by which fibril-associated cytotoxicity, *i.e.* cytotoxicity caused by fibrils themselves or by species dynamically associated with fibrils through direct exchange, could be enhanced. These results not only demonstrate the cytotoxic potential associated with fibrillar samples, but more importantly, reveal that fibril breakage can enhance toxic responses in cells, even for fibrils that have identical molecular architecture. Fibril fragmentation therefore poses a double threat in amyloid disease, providing a mechanism by which fibril load can be rapidly increased, as well as a route by which amyloid cytotoxicity may be enhanced. The results may provide a rationale of the varied cellular responses to fibrils of apparently identical chemical composition and suggest that targeting amyloid fibril stability against breakage may be a powerful strategy for developing therapies against amyloid disease.

EXPERIMENTAL PROCEDURES

Fibril Sample Preparations—All mechanical agitation experiments were performed by stirring 500 μl of fibril samples in 1.5-ml glass vials, each containing a 3 × 8-mm polytetrafluoroethylene-coated magnetic stirring bar. Agitation was performed using a custom-made precision stirrer with accurate rpm readout provided by a revolution counter on the rotor axis (custom-built by the workshop of the School of Physics and Astronomy, University of Leeds) at 1,000 rpm, 25 °C.

Preparation of β_2m fibrils was performed by dissolving lyophilized protein (wild-type β_2m expressed and purified as described previously (3, 24)) into the reaction buffer containing 10 mM sodium dihydrogen phosphate and 50 mM NaCl, adjusted to pH 2.0 using HCl. The reaction mixture was immediately syringe-filtered (0.2-μm Minisart fast flow, Sartorious Stedim Biotech) and split into two equal aliquots. The first aliquot was stirred as described above for 3 days at 25 °C. Under this condition, short fragmented fibrils (LS_{Sh}) form. Long fibrils (LS_{Ln}) were subsequently grown by seeding the second aliquot of β_2m monomers with 0.1% (w/w) of LS_{Sh} fibrils and incubating the mixture at 25 °C under quiescent conditions for 48 h. The agitation sample series were next prepared by stirring the LS_{Ln} fibril sample in a new glass vial. Small sample aliquots were taken after different times of stirring with a dead time of 9 min between the start of the stirring and the first sample taken. Fibrillar aggregates of β_2m with worm-like (WL) or rod-like (RL) morphology (3) were assembled in 150 mM or 250 mM ammonium formate buffer adjusted to pH 3.6 using HCl, respectively (3, 25). The protein monomer concentration of samples used to form the initial fibril stock solutions was 120 μM, and under the employed conditions, all fibril solutions were translucent without visible turbidity, indicating that the samples contain well dispersed fibrils.

Preparation of lysozyme fibrils was performed by first dissolving lyophilized chicken hen egg white lysozyme (Sigma) into 10 mM HCl. The solution was immediately syringe-filtered (0.2-μm MiniSart fast flow) and incubated at 60 °C for 48 h under quiescent conditions. The solution was next placed at 25 °C and left quiescently for ~2 months until fibrils (Lyz_{Ln}) appeared. Fragmented fibrils (Lyz_{Sh}) were obtained by subsequently stirring an aliquot of the fibril sample at 1,000 rpm for 72 h. The protein monomer concentration was 350 μM.

Preparation of α-synuclein fibrils (αSyn) was performed by first dissolving lyophilized protein powder (wild-type αSyn expressed and purified as described in Ref. 26) into 25 mM sodium phosphate buffer at pH 7.5. The sample solution (αSyn_{Ln}) was then incubated under gentle orbital shaking (200 rpm in a 1.5-ml Eppendorf tube) at 37 °C for 1 week and subsequently left quiescently for ~2 months. Short fragmented fibrils (αSyn_{Sh}) were again obtained by stirring of an aliquot of the fibril sample at 1,000 rpm for 72 h. The protein monomer concentration was 350 μM.

Fibril Imaging Using TM-AFM and Negative Stain Electron Microscopy (EM)—For TM-AFM, the β_2m fibrils were imaged using a Dimension 3100 scanning probe microscope (Veeco Instruments) and PPP-NCLR silicon cantilever probes (NanoWorld AG, NANOSENSORS, Neuchatel, Switzerland) with nominal force constant of 48 newtons/m. For LS fibril samples, each sample was diluted to 0.4 μM with sterile filtered deionized water and 20 μl incubated on the surface of freshly cleaved mica for 5 min. The surface was then washed with 1 ml of sterile filtered deionized water and dried under a gentle stream of N_2 gas. For WL and RL fibril samples, the same volume and concentration of the sample material was incubated on the mica surface for 1 min but otherwise using the same protocol. Images of 10 × 10 μm at 1,024 × 1,024 pixels were collected. Negative stain EM imaging was performed as described previously (24).

AFM Data Processing—The AFM images were processed using automated scripts written in MATLAB (MathWorks). For each image, fibril contours were picked out automatically by the scripts to ensure objective analysis. The length of the individual fibrils, as well as the height information of each pixel along the highest ridge of each fibril, was extracted for fibrils that could be unambiguously recognized by the scripts. The resulting distribution of lengths was biased toward shorter fibrils, because longer fibrils are cut off more frequently by image boundaries, by overlap with other fibrils, and by length-dependent differences in surface deposition efficiency of fibrils with different length (27). To correct for this bias, the length distribution was adjusted by factoring in an empirical power function obtained by assuming that the average total length of fibrils recognized on each image should be constant (described in Ref. 27), as expected from the fact that all images are collected on surfaces treated with samples formed from an identical protein monomer concentration, using an identical protocol (27).

From the bias-corrected length distributions, weight average lengths (referred to as the average length throughout this report) were calculated. The results from the fibril extension assay and the liposome dye release assay *versus* the average lengths, proportional to the surface area parallel to the fibril axis per fibril, were fitted to a power law function ($y = ax^b$)

using the total least squares method (28) that takes into account variations in x and y values.

Fourier Transform Infrared (FTIR) Spectroscopy—Fibril samples for FTIR were prepared as described above but using buffer solutions made up using 99.8% D_2O. The pD was adjusted using DCl. The samples were concentrated 10 times by centrifuging a 500-μl sample at 16,300 $\times$ *g* for 2 h and subsequent resuspension to 50 μl using the supernatant. Transmission mode FTIR absorbance spectra of the samples as well as the buffer and the vapor spectra were collected on a Thermo-Nicolet IR-560 (Thermo Scientific) FTIR spectrometer at 25 °C. For each sample, 1,024 scans were obtained at a spectral resolution of 1 cm^{-1}, through a sample path length of 0.05 mm. The final spectra were corrected for the buffer and the vapor signals, and secondary derivatives of the absorbance spectra were calculated and plotted.

Fibril Growth Kinetics Followed by Thioflavin T (ThT) Fluorescence—The fibril growth kinetics of β_2m LS_{Sh} fibrils were monitored using a sample contained within a 1.5-ml glass vial in the same buffer condition and stirred as described above at a protein monomer concentration of 60 μM. A 10-μl sample was removed periodically and diluted into 10 mM sodium phosphate buffer at pH 2.0 with 50 mM NaCl and 10 μM ThT to a final volume of 200 μl. The fluorescence emission of ThT at 480 nm was then read at an excitation wavelength of 440 nm on a PTI QuantaMaster spectrometer (Photon Technology International). An additional 10 μl of the sample was also taken and used for liposome dye release assays at each time point.

For the seeding efficiency assays, the kinetics of 2% (w/w) seeded fibril growth at 12 μM monomer concentration were followed by monitoring the fluorescence of ThT in a 96-well plate using a BMG LABTECH FLUOStar Optima at 25 °C as described previously (29). The initial slope of the resulting growth curves was extracted after normalizing the signals using the baseline signal values and the signal values when the reaction reaches completion. The initial slopes were subsequently used as a measure of the efficiency of fibril samples to seed the growth of new fibrils.

Liposome Dye Release Assay—Large unilamellar vesicles (LUV) were prepared using a lipid mixture containing 1.6 mg/ml phosphatidylcholine and 0.4 mg/ml phosphatidylglycerol purified from chicken egg (Avanti Lipids) to give 20% negatively charged head groups (within typical physiological range (30)). The lipid mixture also contained 0.01 mg/ml rhodamine-labeled phosphatidylethanolamine (Avanti Lipids) for determination of the lipid concentration. The lipids were dissolved in 50 mM HEPES, 10 mM NaCl, 1 mM EDTA, pH 7.4, containing 50 mM carboxyfluorescein (Sigma). LUVs were prepared from the lipid mixture by extrusion through a polycarbonate filter with 400-nm pore size. The LUVs were next washed three times with a buffer (liposome buffer) containing 50 mM HEPES, 107 mM NaCl, 1 mM EDTA, pH 7.4, and resuspended to form a stock solution with final lipid concentration of 0.5 mM. The final stock solution containing LUVs with encapsulated carboxyfluorescein were used within 2 days.

For each dye release assay reaction, 2 μl of the LUV stock solution was diluted with typically 188 μl of liposome buffer. Fibril sample (typically 10 μl) was then added to the solution to give a final volume of 200 μl, and the fluorescence emission of carboxyfluorescein at 513 nm was quantified using an excitation wavelength of 492 nm on a PTI QuantaMaster spectrometer (Photon Technology International). For the concentration series and control experiment with fibril supernatant, fibril samples were diluted prior to addition to the liposome solution with the fibril growth buffer to the final concentrations in monomer equivalents between 12 μM (highest possible concentration for the experiments) and 12 pM for the concentration series and 0.12 μM for the supernatant control. Triplicates were measured for each sample.

The dye release kinetics, with typical traces shown in supplemental Fig. 1*A*, are complex and dependent on factors such as membrane composition. Controls using LUVs composed of 100% phosphatidylcholine, phosphatidylglycerol, phosphatidic acid, or phosphatidylserine all showed dye release (supplemental Fig. 1*B*), demonstrating that disruption of membranes of different composition occurs upon the addition of fibril samples. The kinetic traces of dye release show that the fluorescence signal approaches a plateau after 10 min, which showed less than 100% dye release when compared with liposomes incubated with Triton X-100. Why less than complete dye release occurs is not clear and could be due to a subpopulation of liposomes that are particularly susceptible to dye release, or dye release may be caused by fusion and/or aggregation of liposomes. The fluorescence intensities at 10 min were subsequently chosen as the reporter parameter value for dye release and were recorded and normalized to the signal when liposomes are disintegrated by the addition of 5 μl of a solution containing 20% (v/v) Triton X-100. The low level of background response from buffer was then subtracted from the normalized signals. For comparison between fibrils originating from lysozyme, α-synuclein, and β_2m (see Fig. 6*B*), the relative dye release efficiency for short fibrils in each case was obtained by dividing the dye release efficiency of each sample with that of the corresponding long fibril samples, which had normalized dye release efficiency of 0.48, 0.13, and 0.11, respectively.

Size Exclusion Chromatography—Gel filtration was performed using an analytical Superdex 75 10/300 GL column (GE Healthcare) at 25 °C. All experiments were performed using a running buffer containing 10 mM sodium phosphate, pH 7.0. After the column was equilibrated in the running buffer, 500 μl of a sample (24 μM monomeric β_2m, 12 μM monomer equivalent of LS_{Sh} in liposome buffer, or 12 μM monomer equivalent of LS_{Sh} in liposome buffer incubated at 25 °C for 2 h) each that had been centrifuged at 16,300 $\times$ *g* for 30 min was injected. The flow rate was 0.4 ml/min.

3-(4,5-Dimethylthiazol-2yl)-2,5-diphenyltetrazolium Bromide (MTT) Cell Viability Assay—SH-SY5Y, RAW 264.7 and HeLa cells were cultured in Dulbecco's modified Eagle's medium supplemented with 10% (v/v) fetal bovine serum at 37 °C in 5% CO_2. Cells were plated out at 5,000–7,500 cells/well in 96-well plates (Nunc, Thermo Fisher Scientific or Costar for RAW 264.7 cells) and incubated for 24 h at 37 °C and in 5% CO_2. The medium was then replaced, and the fibril samples or controls (monomeric β_2m, buffer alone, or 0.1% (w/v) NaN_3) were incubated with cells for 24 h at 37 °C and in 5% CO_2. For the β_2m LS fibril samples, the fibrils were concentrated 20-fold into

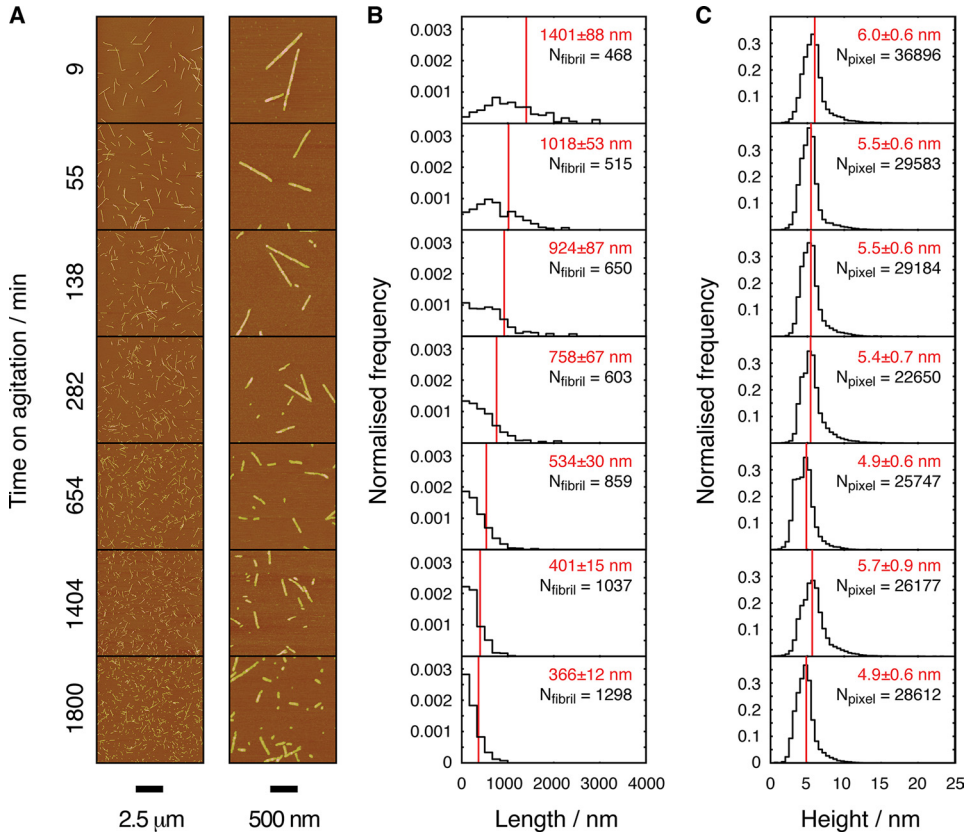

FIGURE 1. **β_2m fibrils agitated to different extents characterized by TM-AFM.** *A*, typical AFM height images of the fibril samples with *scale bars* shown below the images. The *left column* shows whole 1,024 × 1,024 pixel, 10 × 10-μm images. The *right column* shows zoomed in 2 × 2-μm regions of the same images. *B*, normalized frequency (unit area) histograms of the length distribution of each fibril sample. The sample size (N_{fibril}) is indicated in each histogram. The *red text* and *lines* denote the weight average length of each sample with errors corresponding to one S.E. *C*, normalized frequency (unit area) histograms of the height distribution of each fibril sample. The sample size (N_{pixel}) is indicated in each histogram. The *red text* and *lines* denote the modal height values with variations corresponding to one S.D.

sterile filtered deionized water through centrifugation at 16,300 × *g* for 2 h to minimize the impact of the low pH buffer on the cells, and 1 μl was added to each well containing 200 μl of medium. For the β_2m WL samples, the buffer was neutralized using NaOH before addition, and 2 μl was added to each well containing 200 μl of medium. For lysozyme and αSyn samples, 1 μl was added to each well containing 200 of μl medium. After incubation with fibril samples, the medium was replaced, and 20 μl of MTT (5 mg/ml) dissolved in cell medium was incubated with cells for 1.5 h. The medium was discarded, and the resulting formazan crystals were resuspended in dimethyl sulfoxide (DMSO). The absorbance was measured at 570 nm with the signal of background cell debris (measured at 650 nm) subtracted. For each sample, the experiments were repeated on at least three different days with five replicates generally carried out during each day to ensure sufficient sampling of the variations of the experiments for accurate statistical analysis. The results were normalized using the signal for untreated cells as 100% viability and cells treated with NaN_3 as 0% viability. The effect of the added fibril buffer on viability was also subtracted to give the percentage of cell viability of the sample. For comparison between fibrils originating from lysozyme, α-synuclein, and β_2m (see Fig. 6*C*), the relative cell viability in each case was obtained by dividing the viability of cells cultured in each fibril sample with that of cells cultured with long fibril samples, which had a viability of 70, 68, and 82%, respectively.

Antibody Dot Blots—Dot blots of the β_2m samples using WO1 (31) and A11 (9) antibodies were performed according to Ref. 3 except that phosphate-buffered saline (with 0.05% (v/v) Tween 20 for A11 and 0.2% (v/v) Tween 20 for WO1) was used as buffer. Antibody binding was visualized using the Super-Signal West Pico chemiluminescent substrate (Thermo Fisher Scientific, Perbio) and Amersham Biosciences Hyperfilm ECL.

RESULTS

Effect of Mechanical Agitation on the Structural Properties of β_2m Fibrils—To investigate the effects of agitation on the molecular and superstructural properties of amyloid fibrils and to establish whether agitation-promoted fragmentation affects the biological responses of cells to amyloid fibrils, LS fibrils with all the characteristics of amyloid (7) were created *in vitro* from β_2m using well established procedures (29). Samples fragmented to different extents were then generated from a single stock of quiescently grown LS fibrils by mechanical agitation for different lengths of time using a custom-made precision stirrer ("Experimental Procedures"). Each sample was subsequently imaged using TM-AFM. A total of 46 1,024 × 1,024-pixel images, each covering 10 × 10 μm, were collected (Fig. 1*A*). The distributions of fibril length and height in each sample, quantified from the information collected from a total of 5,430 fibrils extracted from the AFM image data using automated scripts (27) are plotted in Fig. 1, *B* and *C*, respectively. The change in average fibril length as a function of the length of time each sample has been agitated is shown in Fig. 2*A*. As shown in Figs. 1*B* and 2*A*, the distribution of the fibril length is shifted toward shorter particles as the duration of time under agitation is increased. The fibril length distribution of the initial sample is broad and shallow with an average length of 1,401 ± 88 nm. After 1,800 min of stirring, a narrower distribution results, with an average length of only 366 ± 12 nm. By contrast, the heights of the fibrils (Fig. 1*C*) remain constant throughout the agitation time (average modal height of 5.2 nm, consistent with previously reported values (3)).

To investigate whether fragmentation induces structural changes in the fibril architecture, the initial and final samples in the agitation time series were analyzed by FTIR spectroscopy (32). The resulting spectra (Fig. 2*B*) show identical

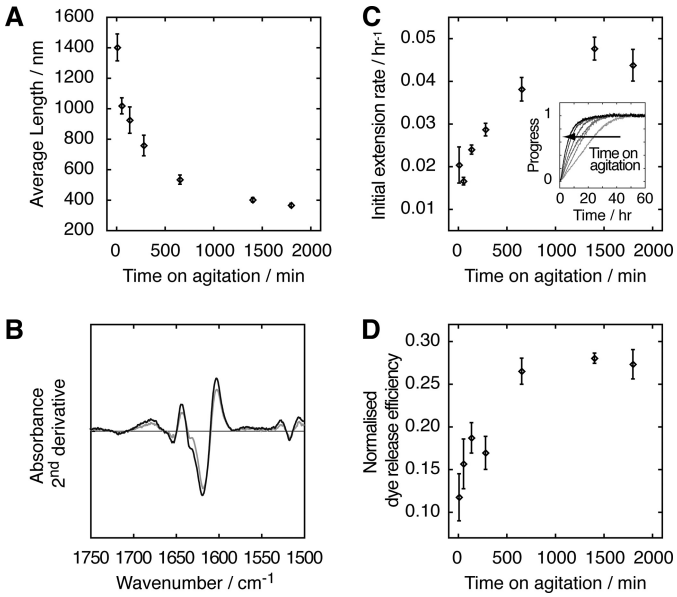

FIGURE 2. **Effect of fibril fragmentation on fibril architecture and the efficiency to seed fibril growth or to cause dye release by liposome membrane disruption.** *A*, weight average length of β_2m fibrils agitated for different length of time. *B*, FTIR spectra of β_2m fibrils before (*gray*) and after 1,800 min of stirring (*black*). The second derivative spectra of the amide I region are shown. *C*, the efficiency of the fibrils to seed new fibril growth characterized by the initial slopes of the normalized fibril elongation traces. The *inset* shows typical normalized kinetic traces of fibril growth monitored by ThT fluorescence at 25 °C with 12 μM β_2m monomer seeded with 2% (w/w) of the fibril samples. The *y* axis indicates the reaction progress. *D*, the efficiency of the fibrils to disrupt liposome membranes of LUVs formed from 80% (w/w) phosphatidylcholine and 20% (w/w) phosphatidylglycerol encapsulated with 50 mM carboxyfluorescein. In *A*, *C*, and *D*, *error bars* represent one S.E.

bands, ruling out significant structural perturbations of the fragmented samples when compared with their longer counterparts, in agreement with previously reported observations by other methods (33). The applied mechanical agitation thus extensively alters the physical attributes of the amyloid fibrils by fragmenting them into shorter units, whereas the molecular architecture of the fibrils remains apparently unperturbed.

Effect of Fibril Fragmentation on the Efficiency of Seeding and Membrane Disruption—Fibril samples from the agitation series were next used in fibril extension assays to probe their ability to seed the growth of new fibrils. In parallel, liposome dye release assays were performed on the same samples to explore the ability of fibrils of different length to disrupt membrane bilayer integrity.

To assay the ability of the fibril samples to seed fibril growth, fresh protein solutions containing 12 μM β_2m monomers were seeded by the addition of 2% (w/w) of each fibril sample from the agitation series, and the initial rate of fibril growth was monitored by measuring the fluorescence of the amyloid-specific dye ThT (Fig. 2*C*). Previous studies have shown that ThT provides an accurate measure of β_2m fibril formation (29). The results showed, as expected, that samples subjected to extensive fragmentation are significantly more efficient in seeding new fibril growth than their less fragmented counterparts (Fig. 2*C*). This response is entirely consistent with an assembly mechanism involving slow nucleation and rapid elongation, as demonstrated for β_2m fibril growth under the conditions employed (29).

Because membrane disruption is a potential generic mechanism associated with the cytotoxicity of amyloid aggregates (see review, Ref. 34), including aggregates formed from β_2m (35, 36), the ability of the fibril samples to disrupt membranes was also assayed by monitoring dye release from LUV formed from 80% phosphatidylcholine and 20% phosphatidylglycerol, within which the fluorescent dye carboxyfluorescein was encapsulated at pH 7.4 ("Experimental Procedures"). When these liposomes were incubated with each fibrillar sample for 10 min, the fluorescence intensity increased considerably (supplemental Fig. 1), indicating that a substantial proportion of the liposomes was disrupted by the presence of the fibrillar material, releasing the encapsulated dye to the bulk solvent and thereby decreasing the self-quenching of fluorescence of the dye in liposome-encapsulated environment. The efficiency by which the fibril samples cause dye release was found to be increased in samples that have experienced most agitation and consequently have a decreased average length (Fig. 2*D*). Although the initial fibril sample that measures 1.4 μm in average length released only ~10% of encapsulated dye, the sample with a measured average length of 366 nm formed by fragmentation for 1,800 min caused a 3-fold increase in dye release over its unagitated counterpart. Thus, despite being indistinguishable in fibril architecture and identical in protein (monomer equivalent) concentration, the samples containing shorter fibrils are better able to disrupt liposome membranes. To further demonstrate the enhanced capability of shorter fibrils to disrupt LUV membranes, an additional experiment was performed in which the dye release caused by a newly fragmented fibril sample agitated for 1,800 min was compared with the dye release capability of the supernatant of exactly the same sample centrifuged at 16,300 × *g* for 30 min. Although the majority of the material in the form of longer fibrils was pelleted by this procedure (21% of total protein material remained in the supernatant after centrifugation), the dye release efficiency of the supernatant was only reduced to 51 ± 2% of the initial sample. This result is consistent with the long fibrils pelleted by centrifugation being less capable of disrupting the liposome membranes than their shorter counterparts remaining in suspension after centrifugation.

Taking all the above data into account, the remarkable picture that emerges is that fibril fragmentation not only increases the efficiency of new fibril growth by seeding, but it also enhances the ability of fibril samples to disrupt liposome membranes. Thus, potentially important new or enhanced biological properties can emerge by shortening amyloid fibrils through fragmentation without other detectable changes to their structural organization.

Cell Viability Reduction in the Presence of Fragmented Fibrils—To determine whether the enhanced ability to disrupt liposome membranes associated with short fibrils is mirrored in a cellular response, the viability of different cell types to the presence of fibril samples formed with or without fragmentation was determined using MTT assays (37). Three different cell lines, human neuroblastoma (SH-SY5Y), mouse macrophage (RAW 264.7), and human cervical carcinoma (HeLa) cells, were each incu-

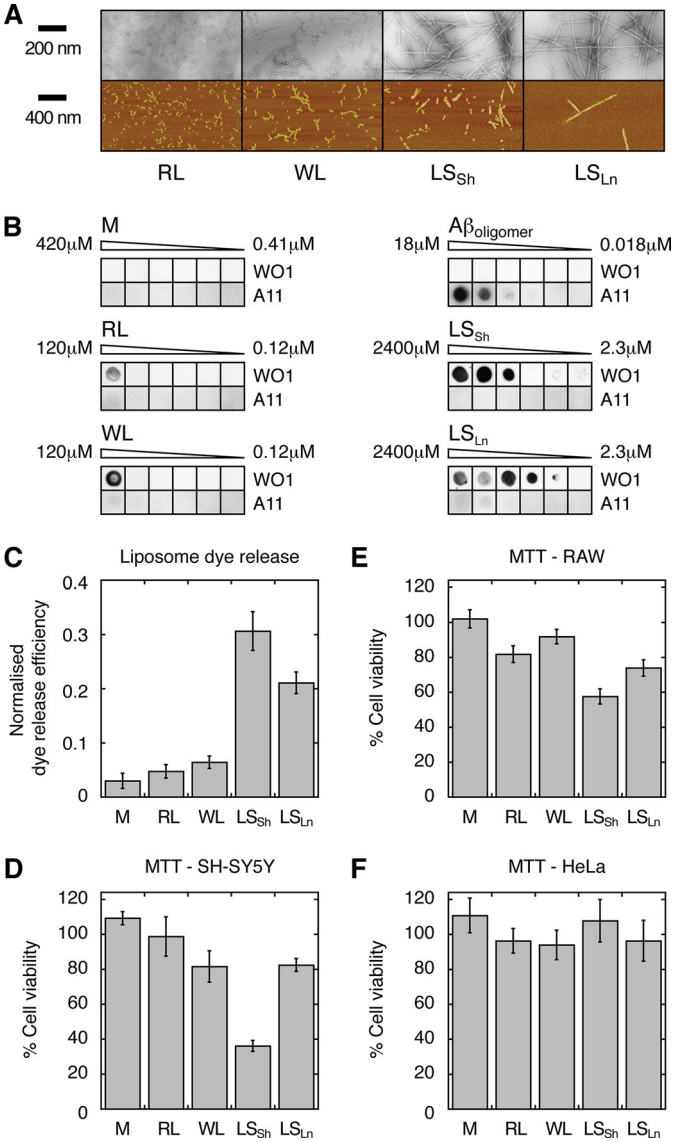

FIGURE 3. **MTT cell viability of different polymeric forms of β_2m.** Assays were performed using monomeric β_2m (*M*) or RL, WL, LS_{Ln}, or LS_{Sh} fibrils formed by stirring LS_{Ln} for 3 days at 1,000 rpm. *A*, different fibril samples used for the MTT assay imaged using negative stain EM (*top images*) and TM-AFM (*lower images*). The *scale bar* for each method is shown to the *left* of the images. *B*, dot blot analysis of the same samples using WO1 (31) or A11 (9) antibodies. The sample concentration (monomer equivalents) tested for each sample is shown above each sample series, with a 4-fold dilution between each sample. Immunoreactivity of A11-positive Aβ oligomers (9) is shown for comparison. *C*, liposome dye release assay of the same samples treated identically to those used for the MTT assays. *D–F*, MTT assays using the same samples with SH-SY5Y, RAW, or HeLa cell lines. In *C–F*, a concentration equivalent to 12 μM monomer was used. The *error bars* in *C–F* indicate one S.E.

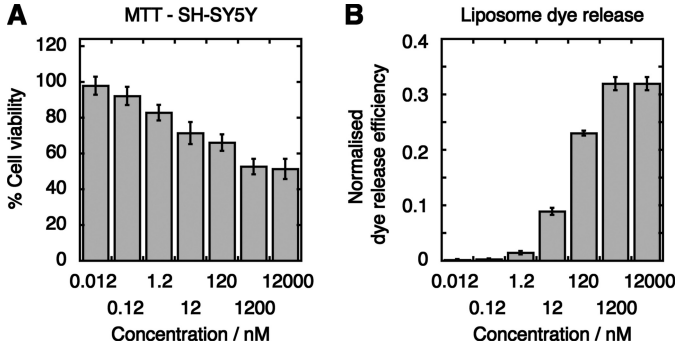

FIGURE 4. **Disruption of liposome membranes and loss of cell viability as a function of the concentration of fragmented fibrils.** *A*, MTT cell viability assay of SH-SY5Y cells incubated with 12 pM to 12 μM monomer equivalent of fragmented LS_{Sh} fibrils. *B*, dye release assay using the same samples. The *error bars* indicate one S.E.

bated with β_2m fibrils (12 μM initial monomer concentration) formed under quiescent conditions (LS_{Ln}, Fig. 3*A*) or with precisely the same fibril sample fragmented by vigorously stirring for 3 days (LS_{Sh}, Fig. 3*A*). Cell viability in the presence of monomeric β_2m, as well as WL, or RL fibrillar aggregates formed from β_2m that have a structure and morphology distinct from the cross-β organization of LS fibrils (3, 38) (Fig. 3*A*) and were formed under different solution conditions at the same monomer concentration, were also assayed for comparison. All fibrillar samples were bound by the WO1 antibody (31) (Fig. 3*B*), which recognizes a generic structural epitope in amyloid fibrils, confirming the presence of fibrillar material. By contrast, no binding by the amyloid oligomer-specific antibody A11 (9) was observed for any of the samples under the protein (monomer equivalent) concentration employed in the MTT assays (12 μM) when compared with strong binding to the A11-positive Aβ oligomers at >5 μM (Fig. 3*B*). The exact same samples used for MTT assays were also used in liposome dye release experiments for direct comparison (Fig. 3*C*). The results of MTT cell viability assays (Fig. 3, *D–F*), from data collected on at least three different days with five replicates within each day show that the cell lines respond differently to the presence of fibril samples in the growth medium, with SH-SY5Y cells showing most sensitivity to the fragmented LS_{Sh} fibril sample, whereas the RAW264.7 cells also showed the largest reduction in cell viability in the presence of LS_{Sh} fibrils (Fig. 3, *D* and *E*). The viability of HeLa cells was not affected by any fibril sample (Fig. 3*F*). Importantly however, for both RAW264.7 and SH-SY5Y cells, cell viability is diminished most markedly when the cells are incubated in the presence of the LS_{Sh} fibril sample, whereas considerably less cytotoxicity is associated with its longer counterparts LS_{Ln} (Fig. 3, *D* and *E*). The dye release experiments also showed a higher level of membrane disruption for the LS_{Sh} fibril sample when compared with LS_{Ln} (Fig. 3*C*). Incubation in the presence of monomeric β_2m, WL, or RL fibrils resulted in no effect or only a minor decrease in cell viability when compared with the effect of the LS_{Sh} fibril sample (Fig. 3, *D–F*) in all of the tested cell lines. In addition, these samples did not result in major membrane disruption when compared with both the LS_{Sh} and the LS_{Ln} fibril samples (Fig. 3*C*).

To further confirm the observed cytotoxic effect associated with the LS_{Sh} fibril sample, the dependence of cell viability of SH-SY5Y cells on the concentration of LS_{Sh} fibrils was determined. The resulting data (Fig. 4*A*) revealed that treatment with the LS_{Sh} fibril sample resulted in decrease in cell viability in a dose-dependent manner down to concentrations in the nM range (monomer equivalent). Liposome dye release experiments performed in parallel on the same samples also showed a similar dose-dependent response (Fig. 4*B*). These results corroborate the finding that the capacity to disrupt liposome membranes and to reduce cell viability is enhanced for the LS_{Sh} fibril sample. Thus, the cytotoxic potential associated with LS fibrils may be mediated by disruptive interactions with cellular mem-

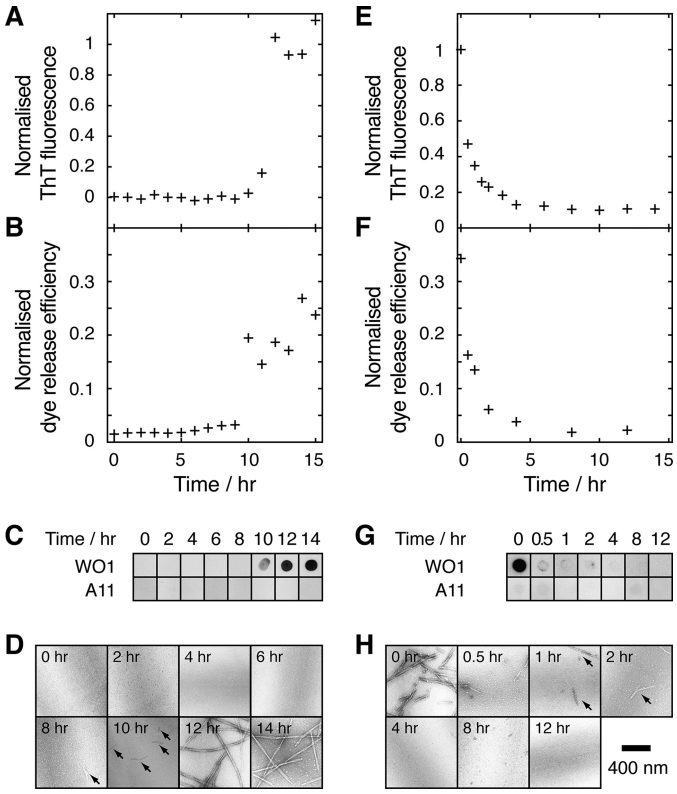

FIGURE 5. **Fibril formation and depolymerization time course.** *A–C*, ThT fluorescence (*A*), dye release assay (*B*), dot blot analysis using the WO1 (31) and A11 (9) antibodies (*C*); and negative stain EM of samples taken during agitated fibril growth at 25 °C, pH 2.0, and 1,000 rpm stirring (*D*). *E–G*, ThT fluorescence (*E*), dye release assay (*F*), dot blot analysis using the WO1 (31) and A11 (9) antibodies (*G*), and negative stain EM of samples taken during fibril depolymerization at 25 °C, pH 7.4, under quiescent conditions (*H*). For EM images in *D* and *H*, the *scale bar* is shown in the *lower right*, and *arrows* indicate the location of fibrils in samples scarcely populated with fibrils.

branes, which are dependent on the physical length of the fibrils within each sample.

Analysis of Membrane Disruption by Species Formed during Fibril Formation and Depolymerization—The results above suggest that considerable disruption to membrane bilayers is associated with LS fibril samples and is enhanced when short fibrils are predominantly populated. Prefibrillar oligomeric species, up to tetramers in size, have been shown to be populated during the lag phase of the assembly of LS β_2m fibrils under the conditions employed (25). It thus remains possible that the residual presence of such oligomeric species in solution at the end of fibril growth that is undetectable by the oligomer-specific antibody A11 may contribute to the observed effects of fibril samples on bilayer integrity. To investigate this possibility, dye release assays were performed during the course of unseeded fibril growth. In parallel, to determine whether fibril depolymerization can generate species capable of membrane disruption, LS_{Sh} fibrils were placed under conditions in which they are unstable, and dye release assays were performed as function of the depolymerization time course.

Fig. 5*A* shows the kinetics of β_2m fibril formation at pH 2.0 monitored by ThT fluorescence. As expected for a fibril growth reaction under agitated conditions wherein fibril fragmentation is a significant secondary process (29), a sigmoidal kinetic trace results that has an extended lag phase and a high apparent rate of elongation. Fig. 5*B* shows the liposome dye release efficiency during the same fibril growth. The data show that the dye release efficiency closely mirrors that of the ThT trace, with significant membrane disruption occurring only when fibrils are formed as judged by WO1 binding, ThT fluorescence, and negative stain EM. Most importantly, no significant membrane disruption is detected during the lag phase where oligomers are most populated (up to 25% mass of the initial monomers), as demonstrated using analytical ultracentrifugation, mass spectrometry (25), and mechanistic modeling (29). Further experiments showed that no fibrils are present during the lag phase, when samples were probed with the amyloid-specific antibody WO1 (Fig. 5*C*) and imaged using negative stain EM (Fig. 5*D*), and no A11 immunoreactivity was observed at any stage during fibril growth (Fig. 5*C*). This excludes the possibility that prefibrillar oligomers are the cause of dye release in this case and instead attribute the presence of species capable of membrane disruption to the time at which LS fibrils first appear. To further confirm that the presence of LS fibrils is responsible for membrane disruption, dye release was also measured during the depolymerization of the LS_{Sh} fibrils induced by altering the pH from the acidic pH of fibril growth to neutral pH (Fig. 5, *E–H*). The experiments revealed that the dye release efficiency decreases (Fig. 5*F*) during fibril depolymerization in a manner that closely mirrors the decrease in the amount of fibrils remaining as monitored by ThT fluorescence (Fig. 5*E*), WO1 immunoreactivity (Fig. 5*G*), and negative stain EM (Fig. 5*H*). No observable A11 immunoreactivity was detected during the time course, demonstrating that fibril depolymerization does not release oligomeric species that are recognized by the A11 antibody. To rule out the presence of persistent species that are not detected by the A11 antibody as the cause of membrane disruption, size exclusion chromatography was performed on samples containing monomeric β_2m, LS_{Sh} fibrils, and LS_{Sh} fibrils depolymerized for 2 h. None of the samples showed any detectable peaks between the void volume and the peak of monomeric β_2m and, more importantly, none of the fractions collected between the void volume and the peak of monomeric β_2m were able to cause any dye release (supplemental Fig. 2). Additional control experiments also showed that the presence of liposomes does not affect the rate of fibril depolymerization. Overall, therefore, the data suggest that the disruption of membrane bilayers is caused by the presence of the short fragmented LS fibrils, either directed by fibrils themselves or through species in direct exchange with fibrils that are distinct from prefibrillar oligomers populated in the lag phase of assembly. Because no persistent oligomers were observed during fibril depolymerization, such species are also unlikely culprits of the membrane disruption effects observed.

Generic Dependence of Cytotoxicity on Fibril Fragmentation—To investigate whether the fragmentation-dependent cytotoxicity associated with β_2m fibrils is observed for amyloid fibrils formed from different proteins that polymerize under different conditions, liposome dye release experiments and MTT cell viability assays were performed on fibrils formed from hen egg white lysozyme and human α-synuclein (see "Experimental Procedures"). Identical to the experiments performed on LS β_2m fibrils, precisely the same fibrils before and after extensive

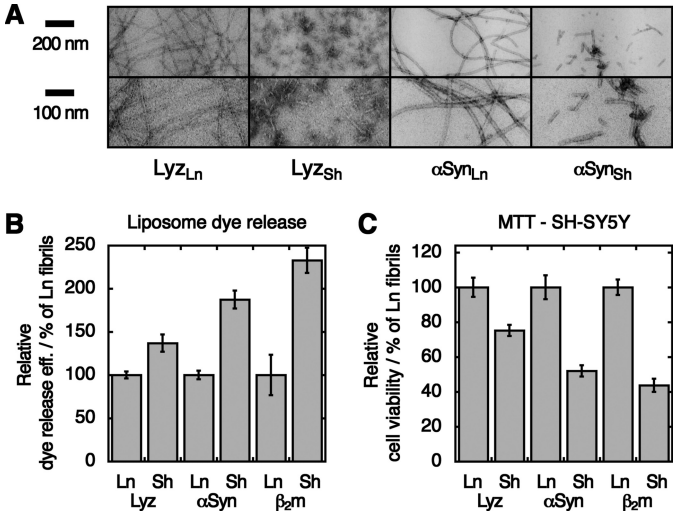

FIGURE 6. **Liposome dye release and MTT assays using fibrils formed from lysozyme (Lyz$_{Ln}$) and α-synuclein (αSyn$_{Ln}$) as well as the same fibrils fragmented by stirring for 3 days at 1,000 rpm (Lyz$_{Sh}$ and αSyn$_{Sh}$).** *A*, negative stain EM images of the fibril samples, with *scale bars* to the *left* of the images. The *lower images* are 2× magnifications of the *upper images*. *B*, liposome dye release assays; *C*, MTT assays using the same fibril samples. In *B* and *C*, the relative signal when compared with that of long fibril samples of each fibril type is plotted to facilitate comparison (see "Experimental Procedures"). Results obtained with fibrils formed by β_2m using the same data as shown in Fig. 3 are included for comparison. The *error bars* indicate one S.E.

fragmentation by agitation were examined (Fig. 6*A*). Strikingly, fibril samples of both α-synuclein and lysozyme are able to disrupt liposome membranes, and in both cases, the dye release efficiency is enhanced for the fragmented fibril samples (Fig. 6*B*). In addition, for all protein fibrils tested, the presence of shortened fibrils resulted in decreased cell viability when compared with their longer counterparts (Fig. 6*C*). These results therefore suggest that fibril fragmentation may provide a generic mechanism of enhancing cytotoxicity associated with amyloid disease.

DISCUSSION

Role of Physical Dimension in Defining the Biological Properties of Amyloid—The results presented here demonstrate that the biological properties of amyloid fibrils depend critically on their length, without the need for parallel changes in their molecular structure or chemical composition. Through the application of carefully controlled fragmentation by mechanical agitation, we show a remarkable correlation between the pathogenic potential of amyloid fibrils and their average length, with fibril samples of decreased average length displaying an enhanced ability to disrupt membrane bilayers and to decrease cell viability when compared with identical fibrils of longer length. Importantly, enhancement of fibril-associated cytotoxicity by fragmentation is not only observed for β_2m fibrils but is also found for fibrils formed from lysozyme and α-synuclein, suggesting that a dependence of cytotoxicity on physical properties such as length is a shared property of these amyloid samples.

The length-dependent fibril-associated cytotoxicity shown here is consistent with the consideration of amyloid aggregates as a nanoscale material in which surface properties and biological availability are critically dependent on their size (22). Akin to man-made or other natural nanoscale materials, amyloid assemblies may present surfaces not normally encountered *in vivo* despite the fact that they are generated *in situ* by physiologically available proteins or peptides. Furthermore, similar to man-made nanomaterials that have been shown to adsorb proteins onto their surfaces (*e.g.* Refs. 39 and 40), amyloid fibrils may perturb biological functions through unintended surface-mediated interactions with membranes, proteins, or other macromolecules. Because the type and the strength of surface-mediated interactions are dependent on the dimensions of the aggregates, amyloid species of different size may give rise to aberrant interactions of different type or biological responses of different magnitude. This size-dependent complexity may contribute to the variability in pathogenic properties of seemingly identical amyloid aggregates formed by the same polypeptide sequence when assessed *in vitro* and in disease associated with the aggregation of the same protein sequence in different individuals.

Role of Fibril Surfaces in Determining Their Biological Properties—We have demonstrated in the present study that LS fibrils of β_2m formed *in vitro* are associated with cytotoxicity in certain cell types in a manner that is dependent on their average length. The fibril samples were further found to be able to disrupt model membrane bilayers in LUVs in a manner that is also dependent on their average length. Through detailed kinetic analysis, the possibility that toxicity results from residual populations of prefibrillar oligomers that are formed during the lag phase of assembly (25, 29) or from persistent oligomers generated during fibril depolymerization could be ruled out. The combined results therefore suggest that the observed cytotoxicity of the fibril samples is fibril-associated, *i.e.* the fibrils themselves, or species in direct dynamic exchange with fibrils, are toxic to cells. The observed enhancement in cytotoxic response for fibrils of short average length could result from a decrease in fibril-fibril interactions and/or an increase in fibril-membrane interactions.

The physical consequences of fibril fragmentation are to decrease the length of individual fibrils and to increase the number of fibrillar particles. These changes lead to a decrease in the surface area parallel to long axis of each fibril and an increase in the total surface area of fibril ends. To decouple the contributions of these different features on the biological effects observed, the scaling relationship between the ability of fibril samples to seed fibril growth or to disrupt liposome integrity and the average fibril length was analyzed (Fig. 7). *Solid black lines* in Fig. 7 show the total least squares fits (28) of a power law function ($y = ax^b$) to the initial fibril extension rate or the dye release efficiency *versus* the average fibril length (proportional to the surface area parallel to the fibril axis per fibril). In the case of initial fibril extension rate *versus* average fibril length (Fig. 7, *A*, *C*, and *E*), the fit resulted in a scaling exponent, $b = -0.95 \pm 0.23$. Fitting with the exponent fixed at -1 did not result in large changes in the quality of the fit. This analysis shows quantitatively that the observed rate of fibril extension is proportional to 1/average fibril length (characterizing the relative number of fibrils, proportional to the total surface area presented by fibril ends). Fibril extension therefore depends on the number of specific extension sites located on fibril ends

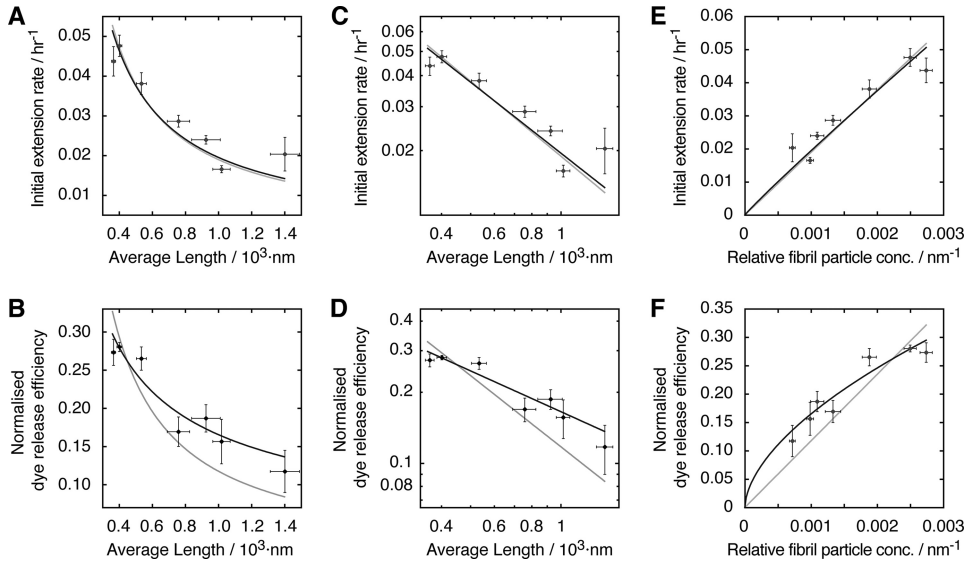

FIGURE 7. **Analyses of the scaling relationships between the ability of the fibril samples agitated for different length of time to seed fibril growth or to disrupt liposome membranes and the average fibril length.** The weight average length is plotted against the initial fibril extension rate (*A*) or the efficiency of the sample to cause membrane disruption measured by release of carboxyfluorescein from LUVs formed from 80% (w/w) phosphatidylcholine and 20% (w/w) phosphatidylglycerol encapsulated with 50 mM carboxyfluorescein (*B*). The *black lines* indicate total least squares fits (28) of a power law function $y = ax^b$, and the *gray lines* indicate the same fits but with the exponent b fixed to −1, which correspond to the case when the initial fibril extension rate or the membrane disruption efficiency is proportional to 1/average fibril length. *Plots C* and *D* represent exactly the same data and fits as *A* and *B*, respectively, but are plotted with logarithmic *x* and *y* axes to visualize the exponent parameter values of the fitted power laws as slopes. *Plots E* and *F* also represent exactly the same data and fits as *A* and *B* but using 1/average fibril length proportional to the fibril particle concentration (*conc.*) as the *x* axis to visualize the relationship between the number of fibrils and the observed seeding or membrane disruption potential of the fibril samples. The *error bars* indicate one S.E.

(Fig. 7*E*), precisely as predicted by the nucleated assembly model with monomer addition (29). The same type of analysis with the dye release efficiency data yielded a scaling exponent of -0.57 ± 0.08, and fitting with the exponent fixed at −1 resulted in large systematic deviations between the fit and the data (Fig. 7, *B*, *D*, and *F*). This result indicates a more complex relationship between dye release efficiency and average fibril length than can be described solely by the increase in the number of fibrils as fragmentation proceeds (Fig. 7*F*). The complexity of the relationship between dye release and the number of fibrils is evident, for example, in that the fibril particle concentration of the LS_{Ln} sample is less than 10 times lower than the LS_{Sh} sample because the average length of LS_{Ln} is less than 10 times longer than LS_{Sh} (Fig. 7), yet a 10-fold decrease in LS_{Sh} concentration (*i.e.* 1.2 μM instead of 12 μM monomer equivalent of LS_{Sh}) does not lead to a corresponding decrease in membrane disruption efficiency, as seen in Fig. 4. Thus, a sample with long fibrils produces a lower level of membrane disruption under the conditions employed than a sample containing the same number of short fibrils. The data suggest therefore that the surface presented by fibril ends, increased by fibril fragmentation, is responsible for promoting fibril extension and may also affect membrane disruption, whereas the surface along the fibril long axis, which is decreased within each fibril particle by fragmentation, does not notably influence fibril extension but may be involved in membrane disruption.

Role of Fibril Fragmentation in Amyloid Cytotoxicity and Implications for Amyloid Disease—Numerous investigations have reported that soluble prefibrillar oligomers are the primary cause of toxicity in amyloid disease, whereas fibrils represent the inert end product of amyloid assembly (16, 17). This hypothesis was originally pursued because the amount of Aβ deposits in Alzheimer patients does not fully correlate with cognitive decline (16, 17). This has since been supported by the correlation found between cognitive and memory decline in Alzheimer disease sufferers and the amount of oligomers present and the demonstration of oligomer-linked cytotoxicity in various cell lines (9, 11, 12, 41). However, by contrast with these observations, other studies have shown that fibrils may yet cause cytotoxicity (13, 15, 18). Recent reports have suggested several different mechanisms of fibril-associated cytotoxicity: by fibrils being cytotoxic themselves (13, 15); by the growth process of fibrillation causing toxicity (21, 42); by fibrils being a source of cytotoxic species that are in dynamic equilibrium with fibril ends (43); or by fibrils being a source of cytotoxic species as a consequence of their depolymerization caused by interaction with lipids (14). For all these possible modes of fibril-associated cytotoxicity, fibril fragmentation could represent an important aspect of amyloid disease, with the average length of fibrils presenting an important parameter, in defining the extent of cytotoxicity observed (schematic illustration in Fig. 8). Thus, by enhancing fibril-membrane surface interactions and/or reducing fibril-fibril interactions that may decrease the biological availability and surface activity of fibrils, shorter fibrils could display enhanced fibril cytotoxicity when compared with longer fibrils. In addition, reducing the overall fibril size could increase the internalization of fibrils by cells (44) and enhance diffusion, resulting in increased biological availability. Similarly, fragmentation increases the quantity of extension-competent surfaces at fibril ends, leading to an increase in the fibril extension rate, as well as increasing the frequency of exchange with soluble species (43). In all of these scenarios, decreasing fibril length by fragmentation would have the ultimate response of enhancing the capacity to increase fibril load by seed extension, as well as opening the door to new or enhanced biological responses through alteration of the physical properties of fibril particles.

Because physical characteristics such as the average length of fibrils influence the cytotoxicity of amyloid assemblies, understanding the mechanistic factors that cause amyloid fragmentation *in vivo* becomes key to understanding amyloidogenicity itself. We have shown previously (29) that fragmentation is the primary effect of agitation, which subsequently influences the rate of fibrillation reactions (29, 45, 46) and can affect the mor-

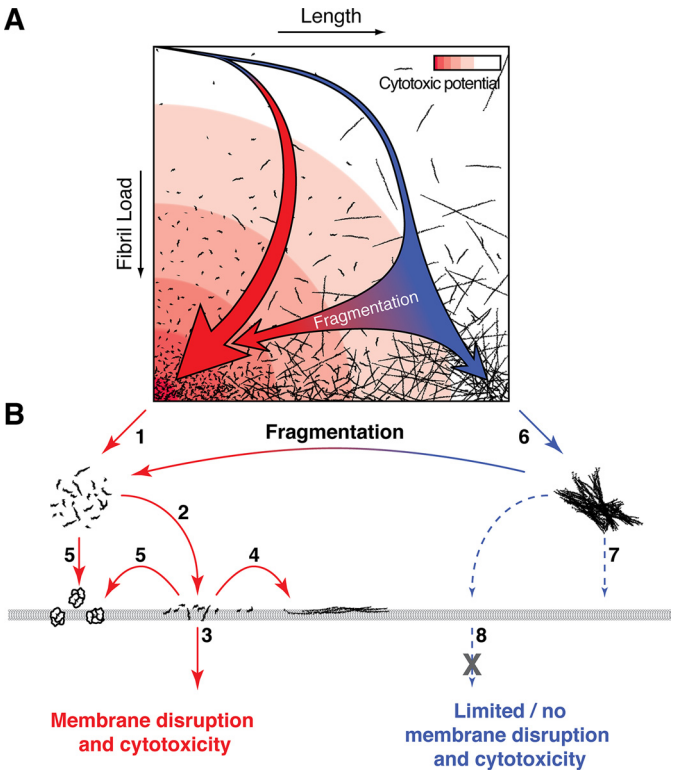

FIGURE 8. **Schematic illustration of the landscape of fibril assembly and fragmentation (*A*) in relation to the mechanism of fibril-associated cytotoxicity (*B*).** In *A*, an assembly landscape is illustrated by fibril load plotted against fibril length. The intensity of the *red background color* represents the cytotoxic potential. The *thick red arrow* in *A* illustrates a representative fibril assembly pathway that would occur in the presence of fibril fragmentation or where nucleation is rapid relative to elongation, resulting in a rapid formation of fibrils with short length distributions. The presence of these short fibrils could lead to enhanced cytotoxicity through decreased fibril-fibril interactions (*B-1* and *B-6*) and increased fibril-membrane interaction (*B-2*). The increased interaction between short fibrils and membrane surfaces could result in membrane damage and a cytotoxic response by fibrils going through the membrane (*B-3*), growing on the membrane surface (*B-4*), or releasing cytotoxic species (*B-5*). The *thin blue arrow* in *A* illustrates a representative fibril assembly pathway when little fibril fragmentation occurs and where nucleation is slow relative to elongation, which results in slow increase of fibril load and the formation of long fibrils. These long fibrils are likely to be less biologically available through increased fibril-fibril interactions (*B-6*), decreased interaction with membranes (*B-7*), and decreased amount of fibrils passing through the membrane (*B-8*) when compared with their short counterparts. Fragmentation after assembly (either mechanical or via chaperones) shortens the average fibril length and thereby enhances the cytotoxic potential without changes to fibril structure (*blue* to *red horizontal arrows* in *A* and *B*).

phology of the fibrils formed from monomers (3, 4). It has also been reported that the phenotype strength of prion strains is dependent on the brittleness of amyloid fibrils in yeast, further supporting the biological importance of fragmentation (47). *In vivo*, fragmentation could be caused by direct mechanical stress, thermal motion, or the activity of chaperones such as Hsp104, which has a known ability to fragment fibril samples (48). Because the stability toward fragmentation may depend critically on the cellular environment, chemically identical amyloid fibrils could provide an array of possibilities *in vivo* for varied phenotypic, toxic, and/or pathogenic properties.

As we have portrayed here using fibrils formed from three different proteins as models of intracellular or extracellular amyloid deposits in disease, fragmentation has a marked effect on the progress of amyloidogenesis. First, fibril fragmentation increases the number of fibril extension sites, hastening the rate of amyloid deposition. Secondly, fragmentation increases the biological availability of fibrillar material and/or increases its interaction with cellular membranes, leading to new/enhanced, deleterious, biological responses. Fibril fragmentation could therefore be a significant generic factor for amyloidosis, providing a double-edged sword by both increasing the fibril load and enhancing the potential for cytotoxicity in parallel. Understanding the changes in biological response invoked by fibril fragmentation will thus become critical in designing therapeutic agents targeting amyloid disease.

Acknowledgments—We thank the members of the Radford and the Homans groups for helpful comments. We thank Charlie Glabe for the generous gift of A11 antibody and Aβ-(1–40) oligomers and Ronald Wetzel for the generous gift of WO1 antibodies. Construction of the stirrer used in this study by the workshop of School of Physics and Astronomy, University of Leeds, is gratefully acknowledged. We also thank Simon Connell for technical help with AFM, Carol Ladner for assistance with FTIR, David Smith for the generous gift of α-synuclein, Toby Tuthill for help with the liposome dye release assay, and Keith Ainley for general technical support.

REFERENCES

1. Chiti, F., and Dobson, C. M. (2006) *Annu. Rev. Biochem.* **75,** 333–366
2. Ferrone, F. A. (1999) *Methods Enzymol.* **309,** 256–274
3. Gosal, W. S., Morten, I. J., Hewitt, E. W., Smith, D. A., Thomson, N. H., and Radford, S. E. (2005) *J. Mol. Biol.* **351,** 850–864
4. Petkova, A. T., Yau, W. M., and Tycko, R. (2006) *Biochemistry* **45,** 498–512
5. van der Wel, P. C., Lewandowski, J. R., and Griffin, R. G. (2007) *J. Am. Chem. Soc.* **129,** 5117–5130
6. Meinhardt, J., Sachse, C., Hortschansky, P., Grigorieff, N., and Fändrich, M. (2009) *J. Mol. Biol.* **386,** 869–877
7. Smith, D. P., Jones, S., Serpell, L. C., Sunde, M., and Radford, S. E. (2003) *J. Mol. Biol.* **330,** 943–954
8. Lee, S., Fernandez, E. J., and Good, T. A. (2007) *Protein Sci.* **16,** 723–732
9. Kayed, R., Head, E., Thompson, J. L., McIntire, T. M., Milton, S. C., Cotman, C. W., and Glabe, C. G. (2003) *Science* **300,** 486–489
10. Reixach, N., Deechongkit, S., Jiang, X., Kelly, J. W., and Buxbaum, J. N. (2004) *Proc. Natl. Acad. Sci. U.S.A.* **101,** 2817–2822
11. Lesné, S., Koh, M. T., Kotilinek, L., Kayed, R., Glabe, C. G., Yang, A., Gallagher, M., and Ashe, K. H. (2006) *Nature* **440,** 352–357
12. Shankar, G. M., Li, S., Mehta, T. H., Garcia-Munoz, A., Shepardson, N. E., Smith, I., Brett, F. M., Farrell, M. A., Rowan, M. J., Lemere, C. A., Regan, C. M., Walsh, D. M., Sabatini, B. L., and Selkoe, D. J. (2008) *Nat. Med.* **14,** 837–842
13. Gharibyan, A. L., Zamotin, V., Yanamandra, K., Moskaleva, O. S., Margulis, B. A., Kostanyan, I. A., and Morozova-Roche, L. A. (2007) *J. Mol. Biol.* **365,** 1337–1349
14. Martins, I. C., Kuperstein, I., Wilkinson, H., Maes, E., Vanbrabant, M., Jonckheere, W., Van Gelder, P., Hartmann, D., D'Hooge, R., De Strooper, B., Schymkowitz, J., and Rousseau, F. (2008) *EMBO J.* **27,** 224–233
15. Meyer-Luehmann, M., Spires-Jones, T. L., Prada, C., Garcia-Alloza, M., de Calignon, A., Rozkalne, A., Koenigsknecht-Talboo, J., Holtzman, D. M., Bacskai, B. J., and Hyman, B. T. (2008) *Nature* **451,** 720–724
16. Campbell, A. (2001) *Med. Hypotheses* **56,** 388–391
17. Lee, H. G., Casadesus, G., Zhu, X., Joseph, J. A., Perry, G., and Smith, M. A. (2004) *J. Alzheimers Dis.* **6,** 137–145
18. Pieri, L., Bucciantini, M., Nosi, D., Formigli, L., Savistchenko, J., Melki, R., and Stefani, M. (2006) *J. Biol. Chem.* **281,** 15337–15344
19. Paravastu, A. K., Qahwash, I., Leapman, R. D., Meredith, S. C., and Tycko, R. (2009) *Proc. Natl. Acad. Sci. U.S.A.* **106,** 7443–7448
20. Devanathan, S., Salamon, Z., Lindblom, G., Gröbner, G., and Tollin, G.

(2006) *FEBS J.* **273,** 1389–1402
21. Engel, M. F., Khemtémourian, L., Kleijer, C. C., Meeldijk, H. J., Jacobs, J., Verkleij, A. J., de Kruijff, B., Killian, J. A., and Höppener, J. W. (2008) *Proc. Natl. Acad. Sci. U.S.A.* **105,** 6033–6038
22. Colvin, V. L. (2003) *Nat. Biotechnol.* **21,** 1166–1170
23. Lynch, I., Dawson, K. A., and Linse, S. (2006) *Sci. STKE* **2006,** pe14
24. Kad, N. M., Thomson, N. H., Smith, D. P., Smith, D. A., and Radford, S. E. (2001) *J. Mol. Biol.* **313,** 559–571
25. Smith, A. M., Jahn, T. R., Ashcroft, A. E., and Radford, S. E. (2006) *J. Mol. Biol.* **364,** 9–19
26. Cappai, R., Leck, S. L., Tew, D. J., Williamson, N. A., Smith, D. P., Galatis, D., Sharples, R. A., Curtain, C. C., Ali, F. E., Cherny, R. A., Culvenor, J. G., Bottomley, S. P., Masters, C. L., Barnham, K. J., and Hill, A. F. (2005) *FASEB J.* **19,** 1377–1379
27. Xue, W. F., Homans, S. W., and Radford, S. E. (2009) *Protein Eng. Des. Sel.* **22,** 489–496
28. Press, W. H. (2002) *Numerical Recipes in C++: The Art of Scientific Computing*, 2nd Ed., pp. 666–670, Cambridge University Press, Cambridge, UK
29. Xue, W. F., Homans, S. W., and Radford, S. E. (2008) *Proc. Natl. Acad. Sci. U.S.A.* **105,** 8926–8931
30. Knight, J. D., and Miranker, A. D. (2004) *J. Mol. Biol.* **341,** 1175–1187
31. O'Nuallain, B., and Wetzel, R. (2002) *Proc. Natl. Acad. Sci. U.S.A.* **99,** 1485–1490
32. Fabian, H., Gast, K., Laue, M., Misselwitz, R., Uchanska-Ziegler, B., Ziegler, A., and Naumann, D. (2008) *Biochemistry* **47,** 6895–6906
33. Lee, Y. H., Chatani, E., Sasahara, K., Naiki, H., and Goto, Y. (2009) *J. Biol. Chem.* **284,** 2169–2175
34. Glabe, C. G. (2006) *Neurobiol. Aging* **27,** 570–575
35. Giorgetti, S., Raimondi, S., Cassinelli, S., Bucciantini, M., Stefani, M., Gregorini, G., Albonico, G., Moratti, R., Montagna, G., Stoppini, M., and Bellotti, V. (2009) *Nephrol. Dial. Transplant.* **24,** 1176–1181
36. Hirakura, Y., and Kagan, B. L. (2001) *Amyloid* **8,** 94–100
37. Mosmann, T. (1983) *J. Immunol. Methods* **65,** 55–63
38. Jahn, T. R., Tennent, G. A., and Radford, S. E. (2008) *J. Biol. Chem.* **283,** 17279–17286
39. Cedervall, T., Lynch, I., Lindman, S., Berggård, T., Thulin, E., Nilsson, H., Dawson, K. A., and Linse, S. (2007) *Proc. Natl. Acad. Sci. U.S.A.* **104,** 2050–2055
40. Linse, S., Cabaleiro-Lago, C., Xue, W. F., Lynch, I., Lindman, S., Thulin, E., Radford, S. E., and Dawson, K. A. (2007) *Proc. Natl. Acad. Sci. U.S.A.* **104,** 8691–8696
41. Näslund, J., Haroutunian, V., Mohs, R., Davis, K. L., Davies, P., Greengard, P., and Buxbaum, J. D. (2000) *JAMA* **283,** 1571–1577
42. Friedman, R., Pellarin, R., and Caflisch, A. (2009) *J. Mol. Biol.* **387,** 407–415
43. Carulla, N., Caddy, G. L., Hall, D. R., Zurdo, J., Gairí, M., Feliz, M., Giralt, E., Robinson, C. V., and Dobson, C. M. (2005) *Nature* **436,** 554–558
44. Morten, I. J., Gosal, W. S., Radford, S. E., and Hewitt, E. W. (2007) *J. Biol. Chem.* **282,** 29691–29700
45. Collins, S. R., Douglass, A., Vale, R. D., and Weissman, J. S. (2004) *PLoS Biol.* **2,** e321
46. Smith, J. F., Knowles, T. P., Dobson, C. M., Macphee, C. E., and Welland, M. E. (2006) *Proc. Natl. Acad. Sci. U.S.A.* **103,** 15806–15811
47. Tanaka, M., Collins, S. R., Toyama, B. H., and Weissman, J. S. (2006) *Nature* **442,** 585–589
48. Shorter, J., and Lindquist, S. (2004) *Science* **304,** 1793–1797